6960 *Inorg. Chem.* **2009**, *48*, 6960–6971
DOI: 10.1021/ic900520j

Inorganic Chemistry
Article

Efficient Catalytic Phosphate Ester Cleavage by Binuclear Zinc(II) Pyrazolate Complexes as Functional Models of Metallophosphatases

Larysa V. Penkova,[†] Anna Maciąg,[§] Elena V. Rybak-Akimova,[‡] Matti Haukka,[#] Vadim A. Pavlenko,[†] Turganbay S. Iskenderov,[¶] Henryk Kozłowski,*[,§] Franc Meyer,*[,∥] and Igor O. Fritsky*[,†]

[†]*Department of Inorganic Chemistry, National Taras Shevchenko University, Volodymyrska str. 64, Kyiv 01033, Ukraine,* [‡]*Department of Chemistry, Pearson Chemistry Laboratory, Tufts University, Medford, Massachusetts 02155,* [∥]*Institut für Anorganische Chemie, Georg-August-Universität Göttingen, Tammannstr. 4, 37077 Göttingen, Germany,* [§]*Faculty of Chemistry, University of Wrocław, 14 F. Joliot-Curie, 50-383 Wrocław, Poland,* [#]*Department of Chemistry, University of Joensuu, P.O. Box 111, 80101, Joensuu, Finland, and* [¶]*Karakalpakian University, Department of Chemistry, Universitet Keshesi 1, 742012 Nukus, Uzbekistan*

Received March 17, 2009

A series of dizinc(II) complexes based on the pyrazolate ligands 3-[(1*E*)-*N*-hydroxyethanimidoyl]-4-methyl-1-*H*-pyrazole-5-carboxylic acid ($\mathbf{H_3L^1}$), (1*E*,1′*E*)-1,1′-(4-methyl-1*H*-pyrazole-3,5-diyl)diethanone dihydrazone ($\mathbf{HL^2}$), (*E*,*E*)-(4-methyl-1*H*-pyrazole-3,5-diyl)bis(methylmethanone) dioxime ($\mathbf{H_3L^3}$), (*E*,*E*)-(4-phenyl-1*H*-pyrazole-3,5-diyl)-bis(phenylmethanone) dioxime ($\mathbf{H_3L^4}$), and 1*H*-pyrazole-3,5-dicarboxylic acid ($\mathbf{H_3L^5}$) have been synthesized and investigated as functional models of phosphoesterases, focusing on correlations between the hydrolytic activity and molecular parameters of the bimetallic core. Speciation of the various dizinc complexes in solution has been determined potentiometrically, and the structures in the solid state have been established by X-ray crystallography. The hydrolysis of two phosphoesters, an RNA model 2-hydroxypropyl-*p*-nitrophenyl phosphate (HPNP) and the pesticide paraoxon-ethyl (POE), promoted by the dinuclear phosphoesterase model complexes has been investigated in DMSO/buffered water (1:1) at 50 °C as a function of complex concentration, substrate concentration, and pH. Drastic differences in the hydrolytic activities of $[Zn_2(\mathbf{HL^1})_2]^0$, $[Zn_2(\mathbf{L^2})_2]^{2+}$, $[Zn_2(\mathbf{H_2L^3})_2]^{2+}$, and $[Zn_2(\mathbf{HL^5})_2]^{2-}$ are observed and can be attributed to molecular peculiarities. Pyrazolate-bridged dinuclear zinc(II) complexes seem to provide a sufficient number of coordination sites for both activating the substrate and generating the nucleophile, where the phosphate esters are preferentially bound in a bidentate bridging fashion (in the case of HPNP) and in a monodentate fashion (in the case of POE).

Introduction

Novel catalysts that are capable of hydrolyzing phosphoesters and carboxylic acid esters under mild conditions have found broad applications across many fields, such as organic synthesis, industrial processes, environmental treatment, and national defense.[1] In particular, agents that promote hydrolysis of phosphoesters could be utilized for decontamination of environmental organophosphate pollutants such as paraoxon.[2] Paraoxon (POE) is a biocide that has been widely used for crop protection. The number of worldwide human intoxications with organophosphate pesticides and insecticides is estimated at 3 000 000/year.[2] Paraoxon is also an analogue of chemical warfare agents such as sarin, soman, and VX,[3] and novel catalysts hydrolyzing organophosphate compounds can be potentially employed for neutralizing such military nerve agents.[4]

Numerous strategies have been examined for cleaving phosphoester and carboxylic ester bonds, and strong acids/bases or metal ion catalysts are usually the reagents of choice for hydrolysis reactions. If applied in organic synthesis, however, extreme pH could be problematic to sensitive functional groups, and some metal complexes may have the drawback of potential toxicity. An alternative strategy is to use hydrolytic enzymes for cleaving ester, amide, and

*To whom correspondence should be addressed. F.M.: tel, +49-551-393012; fax, +49-551-393063; e-mail: franc.meyer@chemie.uni-goettingen.de. H.K.: tel, +48-71-3757251; fax, +48-71-3757251; e-mail. henrykoz@wchuwr.chem.uni.wroc.pl. I.O.F.: tel, +38-044-2393393; fax, +38-044-2393393; e-mail, ifritsky@univ.kiev.ua.

(1) (a) Breslow, R. *Artificial Enzymes*; WILEY-VCH: Weinheim, Germany, 2005. (b) Vahrenkamp, H. *Dalton Trans.* **2007**, *42*, 4751–4759. (c) Zamy, C.; Mazellier, P.; Legube, B. *Int. J. Environ. Anal. Chem.* **2004**, *84*(14−15), 1059–1068. (d) Gómez-Tagle, P.; Yatsimirsky, A. K. *Dalton Trans.* **2001**, 2663–2670.

(2) Eyer, P. *Toxicol. Rev.* **2003**, *22*(3), 165–190.

(3) Steiner, W. E.; Clowers, B. H.; Haigh, P. E.; Hill, H. H. *Anal. Chem.* **2003**, *75*, 6068–6076.

(4) (a) Zheng, Y.; Duanmu, C.; Gao, Y. *Org. Lett.* **2006**, *8*(15), 3215–3217. (b) Wallace, K. J.; Morey, J.; Lynch, V. M.; Anslyn, E. V. *New J. Chem.* **2005**, *29*, 1469–1474. (c) Meyer, F. *Eur. J. Inorg. Chem.* **2006**, 3789–3800.

 Published on Web 06/23/2009

phosphoester bonds. Enzymatic hydrolysis reactions can be carried out at 37 °C in neutral aqueous medium. However, low enzyme stability and high selectivity for native substrates have limited the potential of using hydrolases for practical applications. As a consequence, novel catalysts that can cleave phosphoester and carboxylic ester bonds under mild conditions are still urgently needed.[4]

Currently there is great interest in the design and development of small or medium-sized organic or organometallic compounds as potential therapeutic agents. Those designed to target nucleic acids site-specifically or to mimic the function of enzymes that participate in nucleic acid strand cleavage are of particular interest, because they can lead to safer and more rational approaches to novel therapeutic agents for cancer, viral diseases, and tools for molecular biology.[5,6]

Nature has developed both ribozymes and ribonucleases to achieve rapid, site-specific, and catalytic cleavage of RNA under physiological conditions. Investigations have shown that the 2′-hydroxy function on the RNA ribose makes hydrolysis or transesterfication much faster than that found for DNA, which lacks this important functionality.[7] DNases, RNases, phosphatases, and ribozymes all hydrolyze phosphodiester bonds with the direct participation of one or more metal ion centers, such as Mg(II), Zn(II), and Co(II).[7,8] Various phosphoesterases are known to contain two or even three cooperating zinc ions within their active site.[7,9,10] In many of these, one or more water molecules are directly bound to the metal ion.[4] Synthetic hydrolase models have been very useful in providing information on basic functional principles and mechanistic aspects of enzyme action.[11] In addition, there is hope that artificial nucleases for biomimetic hydrolysis of DNA or RNA will eventually lead to beneficial applications in biotechnology and medicine.[12] Despite the numerous studies, however, there still is only limited knowledge of the factors that govern hydrolytic activity of dizinc(II) arrays and a paucity of general structure−reactivity correlations.[13]

In this paper, we describe the results obtained in the study of zinc(II) complexes of the pyrazolate-based dinucleating ligands 3-[(1*E*)-*N*-hydroxyethanimidoyl]-4-methyl-1*H*-pyrazole-5-carboxylic acid ($\mathbf{H_3L^1}$), (1*E*,1′*E*)-1,1′-(4-methyl-1*H*-pyrazole-3,5-diyl)diethanone dihydrazone ($\mathbf{HL^2}$), (*E*,*E*)-(4-methyl-1*H*-pyrazole-3,5-diyl)bis(methylmethanone) dioxime ($\mathbf{H_3L^3}$), (*E*,*E*)-(4-phenyl-1*H*-pyrazole-3,5-diyl)bis(phenylmethanone) dioxime ($\mathbf{H_3L^4}$), and 1*H*-pyrazole-3,5-dicarboxylic acid ($\mathbf{H_3L^5}$) (Scheme 1) as catalysts of the hydrolysis of two phosphoesters: 2-hydroxypropyl-*p*-nitrophenyl phosphate (HPNP) as an RNA model (Scheme 2) and the pesticide paraoxon-ethyl (POE). Unlike previously reported pyrazolate-based ligands with two chelating arms appended at the 3- and 5-positions,[14] the present ligands bear in these positions arms that contain potentially anionic electron-donor groups having N- and O-donor functions (carboxylic, oxime, and hydrazone). These groups are also able to form hydrogen bonds which can support metal ion coordination and may participate in the generation of an intramolecular hydroxide nucleophile that can be involved in catalytic action. Via such second-sphere interactions the ligands used here may thus improve the efficacy of their complexes as functional enzyme models. In our study, particular attention is devoted to the metal-catalyzed intramolecular transesterification of HPNP, extensively employed as an RNA model substrate, whose mechanism, rather surprisingly, has never been investigated in detail. The reactivity data obtained for the different complexes have been related to the thermodynamic stability and acidity of coordinated water as an essential means to evaluate the factors which control the Zn(II)-catalyzed phosphodi- and phosphotriester hydrolysis.

Experimental Section

Materials and Measurements. Melting points/decomposition temperatures were determined with an OptiMelt system (Stanford Research Systems, Inc.) using open capillaries; the values are uncorrected. ^{1}H and ^{13}C NMR spectra were recorded on a Bruker Avance 500, a Bruker Avance 400, or a Bruker 300 spectrometer. ^{13}C resonances were obtained with broadband proton decoupling; spectra were recorded at 298 K. ^{1}H NMR and ^{13}C NMR chemical shifts were referenced internally to solvent signals. The solvent signal was used as the chemical shift reference (DMSO-d_6; δ_H 2.49, δ_C 39.7). ^{31}P spectra were externally referenced to 85% phosphorous acid. Mass spectra were recorded with a Finnigan MAT 95 (EI), Bruker APEX IV (HRMS, ESI), or AutoFlex Bruker Daltonics instrument (GALDI). IR spectra from KBr pellets were recorded on a Digilab Excalibur Series FTS 3000 spectrometer. Elemental analyses were performed by the analytical laboratory of the Institut für Anorganische Chemie der Universität Göttingen using a Heraeus CHN-O-RAPID instrument or an Elementar vario EL III instrument. UV−vis spectra were recorded with an Analytik Jena Specord 100 spectrometer.

Synthesis. All chemicals were purchased from commercial sources and used as received. Ligands $\mathbf{H_3L^1}$,[15] $\mathbf{H_3L^5}$,[16] and complex $\mathbf{5}$[17] were synthesized according to the reported methods.

Caution! *Although no problems were encountered in this work, transition metal perchlorate complexes are potentially explosive and should be handled with proper precautions.*

(5) (a) Erkkila, K. E.; Odom, D. T.; Barton, J. K. *Chem. Rev.* **1999**, *99*(9), 2777–2796. (b) Eisenwiener, A.; Neuburger, M.; Kaden, T. A. *Dalton Trans.* **2007**, *2*, 218–233.
(6) Kimura, E. *Acc. Chem. Res.* **2001**, *34*(2), 171–179.
(7) (a) Wilcox, D. E. *Chem. Rev.* **1996**, *96*(7), 2435–2458. (b) Mitra, R.; Peters, M. W.; Scott, M. J. *Dalton Trans.* **2007**, *35*, 3924–3935. (c) Mathews, R. A.; Rossiter, C. S.; Morrow, J. R.; Richard, J. P. *Dalton Trans.* **2007**, *34*, 3804–3811. (d) Molenveld, P.; Engbersen, J. F. J.; Kooijman, H.; Spek, A. L.; Reinhoudt, D. N. *J. Am. Chem. Soc.* **1998**, *120*, 6726–6737.
(8) (a) Williams, N. H.; Takasaki, B.; Wall, M.; Chin, J. *Acc. Chem. Res.* **1999**, *32*(6), 485–493. (b) Bonfa, L.; Gatos, M.; Mancin, F.; Tecilla, P.; Tonellato, U. *Inorg. Chem.* **2003**, *42*(12), 3943–3949. (c) Bazzicalupi, C.; Bencini, A.; Bianchi, A.; Fusi, V.; Giorgi, C.; Paoletti, P.; Valtancoli, B.; Zanchi, D. *Inorg. Chem.* **1997**, *36*, 2784–2790.
(9) (a) Sträter, N.; Lipscomb, W. N.; Klabunde, T.; Krebs, B. *Angew. Chem., Int. Ed. Engl.* **1996**, *35*(18), 2024–2055. (b) Fritsky, I. O.; Ott, R.; Pritzkow, H.; Krämer, R. *Chem. Eur. J.* **2001**, *7*(6), 1221–1231.
(10) Horton, N. C.; Perona, J. J. *Nat. Struct. Biol.* **2001**, *8*, 290–293.
(11) Khersonsky, O.; Roodveldt, C.; Tawfik, D. *Curr. Opin. Chem. Biol.* **2006**, *10*(5), 498–508.
(12) Hegg, E. L.; Burstyn, J. N. *Coord. Chem. Rev.* **1998**, *173*(1), 133–165.
(13) (a) Bauer-Siebenlist, B.; Meyer, F.; Farkas, E.; Vidovic, D.; Cuesta-Seijo, J. A.; Herbst-Irmer, R.; Pritzkow, H. *Inorg. Chem.* **2004**, *43*(14), 4189–4202. (b) Bauer-Siebenlist, B.; Meyer, F.; Farkas, E.; Vidovic, D.; Dechert, S. *Chem. Eur. J.* **2005**, *11*, 4349–4360. (c) Yashiro, M.; Kaneiwa, H.; Onaka, K.; Komiyama, M. *Dalton Trans.* **2004**, *4*, 605–610.
(14) (a) Prokofieva, A.; Prikhod'ko, A. I.; Enyedy, E. A.; Farkas, E.; Maringgele, W.; Demeshko, S.; Dechert, S.; Meyer, F. *Inorg. Chem.* **2007**, *46*(10), 4298–4307. (b) Meyer, F. *Eur. J. Inorg. Chem.* **2006**, 3789–3800. (c) Meyer, F.; Pritzkow, H. *Eur. J. Inorg. Chem.* **2005**, 2346–2351.
(15) Wolff, L. *Justus Liebigs Ann. Chem.* **1902**, *325*, 185–186.
(16) Schenck, T.; Milne, C.; Sawyer, J.; Bosnich, B. *Inorg. Chem.* **1985**, *24*, 2334–2337.
(17) Zhang, J.-F.; Li, X.-H. *Acta Crystallogr.* **2006**, *E62*, m125–m127.

Scheme 1. Ligands and Complexes Used in the Present Work

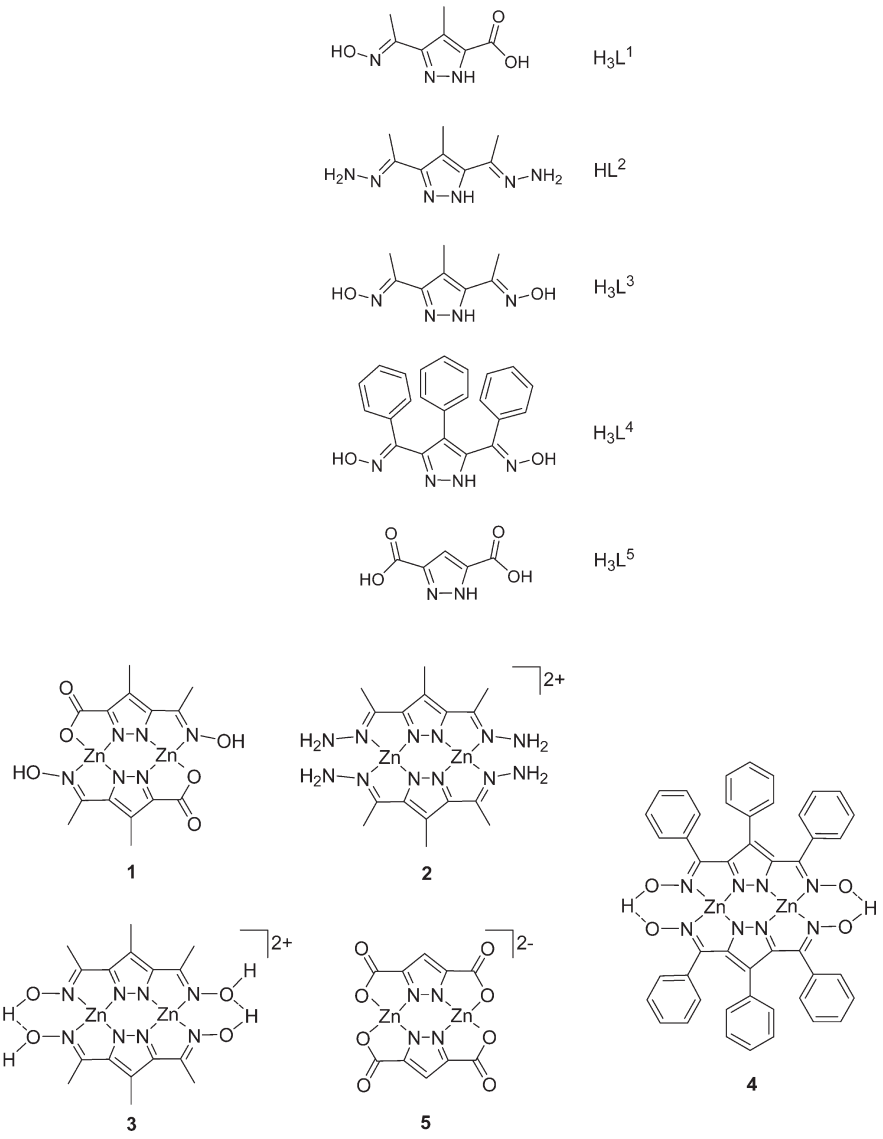

Scheme 2. (a) Hydrolytic Decomposition of Paraoxon-ethyl (POE) and (b) Intramolecular Hydrolytic Degradation of 2-(Hydroxypropyl)-*p*-nitrophenyl Phosphate (HPNP), Resulting in Formation of a Cyclic Phosphate (3-Methyl-2,5-dioxaphospholan-2-ol 2-Oxide) and the *p*-Nitrophenolate Ion

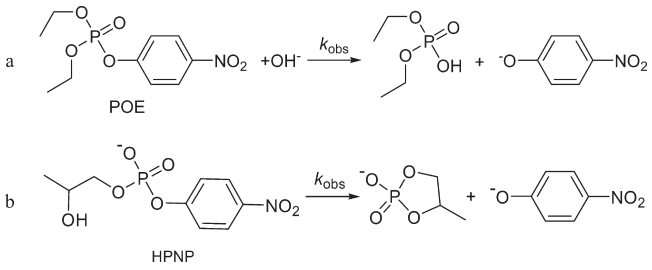

Synthesis of 3-[(1*E*)-*N*-Hydroxyethanimidoyl]-4-methyl-1*H*-pyrazole-5-carboxylic Acid (H_3L^1). 5-Acetyl-4-methyl-1*H*-pyrazole-3-carboxylic acid[18] (3 g, 0.018 mol), $NH_2OH \cdot HCl$ (1.86 g, 0.027 mol), and CH_3COONa (2.80 g, 0.027 mol) were dissolved in water (50 mL). The mixture was stirred for 2 h, and the pH was adjusted to 4 by slow addition of aqueous HCl (1:1). A white precipitate formed. The mixture was left to stand for 10−12 h, and the solid material was separated by filtration and dried under vacuum. Yield: 2.2 g (67%); white solid, mp 220 °C. IR (KBr, cm^{-1}): 1690 ($\nu_{C=N}$) (s), 1640 (m), 1590 (s), 1400 (m), 1370 (m), 1300 (m), 1260 (m), 1240 (s), 1200 (m), 1130 (w), 1070 (w), 1005 (ν_{N-O}) (m), 960 (w), 925 (w), 790 (m), 725 (w), 650 (w). ^1H NMR (500 MHz, DMSO-d_6): δ 2.13 (s, 3H, CH_3), 2.34 (s, 3H, CH_3(Pz)), 11.08 (br, 1H, NOH). ^{13}C NMR (500 MHz, DMSO-d_6): δ 29.9 (CH_3(Pz)); 30.6 (CH_3(ket)); 121.1, 125.6, 129.2 (3C-(Pz)). MS (EI, 70 eV): m/z (%) 182 (75) $[M - H]^+$. Anal. Calcd for $C_7H_9N_3O_3$: C, 45.90; H, 4.95; N, 22.94. Found: C, 45.23; H, 5.36; N, 22.44.

Synthesis of (1*E*,1′*E*)-1,1′-(4-Methyl-1*H*-pyrazole-3,5-diyl) diethanone Dihydrazone (HL^2). 3,5-Diacetyl-4-methyl-1*H*-pyrazole[18] (1 g, 0.006 mol) and $N_2H_4 \cdot H_2O$ (1.2 g, 0.024 mol) were dissolved in methanol (20 mL). One to two drops of acetic acid were added to the solution. The mixture was stirred for 2 h, whereupon a white precipitate formed. This was separated by filtration and dried under vacuum. Yield: 0.95 g (81.7%); white solid, mp 275 °C. IR (KBr, cm^{-1}): 3370 (br, s), 3285 (br, s), 2985 (br, w), 1670 (w), 1605 (m), 1455 (w), 1375 (m), 1320 (br, w), 1295

(18) Sachse, A.; Penkova, L.; Noel, G.; Dechert, S.; Varzatskii, O. A.; Fritsky, I. O.; Meyer, F. *Synthesis* **2008**, *5*, 800–806.

(br, w), 1250 (m), 1200 (m), 1135 (sh), 1100 (m), 1055 (m), 980 (w), 940 (w), 850 (s), 750 (s), 660 (w), 585 (w), 550 (w), 490 (m). ^{1}H NMR (500 MHz, DMSO-d_6): δ 2.00 (s, 6H, CH_3), 2.23 (s, 3H, CH_3(Pz)), 6.18 (s, 4H, NH_2), 12.35 (s, 1H, N(Pz)−H). ^{13}C NMR (500 MHz, DMSO-d_6): δ 11.025 (CH_3(pz)^4), 12.335 (CH_3), 109.393 (C(pz)^4), 155.92 (C(pz)^{3,5}), 195.18 (O=CCH$_3$). MS (EI, 70 eV): m/z (%) 194.0 (100) [M]. Anal. Calcd for $C_8H_{14}N_6$: C, 49.47; H, 7.26; N, 43.27. Found: C, 47.57; H, 7.47; N, 43.62.

Synthesis of (*E*,*E*)-(4-Phenyl-1*H*-pyrazole-3,5-diyl)bis(phenylmethanone) Dioxime (H_3L^4). 3,5-Dibenzoyl-4-phenyl-1*H*-pyrazole[18] (7.05 g, 0.02 mol), $NH_2OH\cdot HCl$ (2.78 g, 0.04 mol), and CH_3COONa (8.32 g, 0.08 mol) were dissolved in a water/methanol (1:1) mixture (100 mL) and stirred for 1 h. $NiCl_2\cdot 6H_2O$ (4.76 Γ, 0.02 mol) was added to the solution, which led to the formation of a yellow precipitate of a putative nickel complex. This was separated by filtration and added to a solution of KCN (8 g) in water/methanol (1:1, 50 mL), and the mixture was boiled for 1 h. The resulting yellow solid of the ligand was separated by filtration and recrystallized from benzene/heptane. Yield: 5.48 g (71.7%); yellow solid, mp 123 °C. IR (KBr, cm^{-1}): 3221 (br, s), 3059 (s), 2855 (m), 1655 ($\nu_{C=N}$) (m), 1600 (w), 1495 (m), 1448 (m), 1290 (m), 1243 (w), 1176 (w), 1080 (w), 1061 (w), 980 (ν_{N-O}) (s), 938 (ν_{N-O}) (s), 768 (s), 695 (vs), 529 (w). ^{1}H NMR (300 MHz, $CDCl_3$): δ 8.22−8.92 (m, 15 H, C*H*(Ar)), 12.76 (br, 1 H, N*H*), 13.30 (br, 1 H, O*H*). 14.71 (br, 1 H, O*H*). ^{13}C NMR (300 MHz, $CDCl_3$): δ 99.54 (C(pz)^4), 119.80 (C(pz)$^{3/5}$), 126.21 (CH(Ar)), 126.79 (CH(Ar)), 127.23 (CH(Ar)), 127.75 (CH(Ar)), 128.46 (CH(Ar)), 129.31 (CH(Ar)), 131.33 (C(Ar)), 132.67 (C(Ar)), 147.11 (C=NOH). ESI-MS: m/z (%) 383.1 (100) [M + H]$^-$. Anal. Calcd for $C_{23}H_{18}N_4O_2$: C, 72.24; H, 4.74; N, 14.65. Found: C, 72.03; H, 5.96; N, 14.44.

[$Zn_2(HL^1)_2(Py)_4$]·2H_2O (1). To a solution of H_3L^1 (0.0458 g, 0.25 mmol) in DMF (2.5 mL) was added a solution of $Zn(NO_3)_2\cdot 6H_2O$ (0.0474 g, 0.25 mmol) in water (2.5 mL), and the mixture was stirred at room temperature for 2 h. The resulting pale yellow solution was filtered and salted out with pyridine to gradually yield pale yellow crystals (99 mg, 94%) of **1**. IR (KBr, cm^{-1}): 3460 (br, s), 1650 ($\nu_{C=N}$) (s), 1640 (sh, s), 1600 (vs), 1480 (w), 1440 (m), 1350 (w), 1310 (m), 1240 (w), 1145 (w), 1070 (w), 1040 (ν_{N-O}) (m), 1010 (w), 950 (w), 835 (w), 820 (w), 790 (w), 760 (m), 705 (m). ^{1}H NMR (400 MHz, DMSO-d_6): δ 2.77 (s, 6H, CH_3(pz)), 2.93 (s, 6H, CH_3), 7.33 (8H, Py), 7.73 (4H, Py), 8.52 (8H, Py). GALDI-MS: m/z 681 [$Zn_2(HL^1)_2$(Py)(DMF)$(H_2O)_2$]$^+$. Anal. Calcd for $C_{34}H_{38}N_{10}O_8Zn_2$: C, 48.30; H, 4.53; N, 16.57. Found: C, 43.71; H, 3.99; N, 17.02.

[$Zn_2(L^2)_2(CH_3COO)_2$]·DMF·2H_2O (2). To a solution of HL^2 (0.014 g, 0.25 mmol) in DMF (2.5 mL) was added a solution of KOH (0.0140 g, 0.25 mmol) in water (2.5 mL), and the mixture was stirred at room temperature for 5 min. Then a solution of $Zn(CH_3COO)_2\cdot 2H_2O$ (0.0459 g, 0.25 mmol) in water (2.5 mL) was added, and stirring was continued at room temperature for 2 h. The resulting pale yellow solution was filtered and slowly allowed to evaporate to gradually yield pale yellow crystals (82 mg, 88%) of the product **2**. IR (KBr, cm^{-1}): 3460 (br, s), 3275 (br, s), 2980 (w), 1640 (w), 1600 (m), 1450 (w), 1380 (m), 1310 (br, w), 1260 (m), 1200 (m), 1130 (sh), 1090 (m), 1050 (m), 970 (w), 755 (vs), 665 (w), 580 (w). ^{1}H NMR (400 MHz, DMSO-d_6): δ 1.98 (s, 6H, CH_3), 2.20 (s, 3H, CH_3^{Pz}), 6.70 (s, 4H, NH_2). GALDI-MS: m/z 680 [$Zn_2(L^2)_2(CH_3COO)_2$] + K$^+$. Anal. Calcd for $C_{23}H_{43}N_{13}O_7Zn_2$: C, 37.11; H, 5.82; N, 24.46. Found: C, 36.88; H, 5.02; N, 24.46.

[$Zn_2(H_2L^3)_2(NO_3)_2$] (3). To a solution of H_3L^3 (0.098 g, 0.5 mmol) in methanol (15 mL) was added a solution of $Zn(NO_3)_2\cdot 6H_2O$ (0.1862 g, 0.5 mmol) in water (2.5 mL), and the mixture was stirred at room temperature for 2 h. The resulting colorless solution was filtered and slowly allowed to evaporate to gradually yield the product **3** as a pale yellow solid (161 mg, 74%). IR (KBr, cm^{-1}): 3432 (br, s), 1630 ($\nu_{C=N}$) (s), 1573 (s), 1384 (vs), 1318 (s), 1229 (m), 1122 (w), 1037 (ν_{N-O}) (m), 960 (m), 820 (w), 773 (w), 697 (w), 623 (w). ^{1}H NMR (400 MHz, DMSO-d_6): δ 1.85 (s, 3H, CH_3(pz)^4), 2.14 (s, 6H, CH_3), 11.26 (br, NOH). GALDI-MS: m/z 644 [$Zn_2(H_2L^3)_2(NO_3)_2$ − H]$^+$. Anal. Calcd for $C_{16}H_{22}N_{10}O_{10}Zn_2$: C, 24.98; H, 2.88; N, 21.85. Found: C, 25.20; H, 2.62; N, 22.07.

[$Zn_2(HL^4)_2$] (4). To a solution of H_3L^4 (0.0765 g, 0.2 mmol) in methanol (5 mL) was added $Zn(ClO_4)_2\cdot 6H_2O$ (0.0745 g, 0.2 mmol), and the mixture was stirred at room temperature for 30 min. The resulting yellow solution was filtered and set aside for slow evaporation at room temperature to yield dark yellow crystals (42 mg, 47%) of the product **2**. IR (KBr, cm^{-1}): 2940 (m), 2870 (m), 1735 (m), 1640 (w), 1605 ($\nu_{C=N}$) (w), 1465 (w), 1390 (m), 1290 (m), 1150 (s), 1120 (ν_{N-O}) (s), 1095 (ν_{N-O}) (s), 920 (w), 750 (w), 700 (m), 665 (m). ^{1}H NMR (400 MHz, DMSO-d_6): δ 6.98−8.14 (m, 15 H, C*H*(Ar)), 11.24 (br, 1 H, O*H*). 12.07 (br, 1 H, O*H*). GALDI-MS: m/z 905.6 [$Zn_2(HL^4)_2$ + H]$^+$. Anal. Calcd for $C_{46}H_{32}N_8O_4Zn_2$: C, 61.97; H, 3.62; N, 12.57. Found: C, 61.61; H, 3.93; N, 12.33.

Kinetic Measurements. The kinetic measurements were performed at 50 °C using buffered solutions in DMSO/water (1:1). MES (2-(*N*-morpholino)ethanesulfonic acid), BES (*N*,*N*-bis(2-hydroxyethyl)-2-aminoethanesulfonic acid), TAPS ([(2-hydroxy-1,1-bis(hydroxymethyl)ethyl)amino]-1-propanesulfonic acid), CHES (2-(*N*-cyclohexylamino)ethanesulfonic acid), and CAPS (3-(cyclohexylamino)-1-propanesulfonic acid) were used as buffers. The ionic strength was fixed at 0.1 M with sodium perchlorate. In a typical experiment, 1.5 mL of aqueous buffer solution was mixed with 0.5 mL of complex stock solution (in DMSO) and 0.5 mL of DMSO in a temperature-controlled spectrophotometric cell. After equilibration for 5 min, 0.5 mL of POE or HPNP stock solution (in DMSO) was added and data collection was started immediately. The cleavage of substrate was monitored by following the increase of the 4-nitrophenolate absorption at 414 nm. The activities of the complexes were determined by the method of initial rates. At least two independent measurements were made. Conversion from absorbance to concentration was performed by using the Lambert−Beer law, $A=\varepsilon_{eff}c$. The pH dependence of ε_{eff} was determined with 4-nitrophenol in the above solvent mixtures.

pH-Metric Titrations. Due to the low solubility of the studied ligands in pure water, all measurements were conducted in a MeOH/H_2O (80:20 w/w) mixture. Ligands and their complexes were also partly soluble in DMSO/H_2O (50:50 w/w), but potentiometric measurements were not possible in that solvent mixture. Potentiometric titrations were performed on a MOLSPIN pH-meter system at a constant temperature of 25 °C under an argon flow using NaOH as titrant and a RUSSEL CMAW 711 standard microcombined glass electrode with its KCl aqueous reference solution replaced with 0.1 M NaCl dissolved in MeOH/H_2O (80:20 w/w). The constant ionic strength was adjusted to 0.1 M by use of sodium perchlorate. The pH meter was calibrated daily in terms of hydrogen ion concentration using $HClO_4$, and a pK_w of 14.42 was established. In the case of ligands HL^2, H_3L^3, and H_3L^4 complexation equilibria could not be studied, due to the very high or very low protonation constants, beyond the accessible pH range.

Titrations of 2 mL solutions of free ligands and their zinc complexes were performed between pH 2 and 10 at different molar ratios. H_3L^5 was titrated within the pH range 2.5−8.0 due to precipitation. Also a 1:1 metal to ligand molar ratio could not be examined potentiometrically due to precipitation. The pH-metric results were used to establish the stoichiometry of formed species, and their stability constants were computed with the help of the SUPERQUAD program.

Crystal Structure Determination. Details of the data collection and processing, structure analysis, and refinement are summarized in Table 1. Diffraction data were collected on a Xcalibur-3 (ω and φ scans) equipped with

Table 1. Crystal Data and Structure Refinement Details for **1**, **2**, and **4**

	1	**2**	**4**
empirical formula	$C_{34}H_{38}N_{10}O_8Zn_2$	$C_{23}H_{43}N_{13}O_7Zn_2$	$C_{46}H_{32}N_8O_4Zn_2$
formula wt	845.48	744.44	891.54
cryst syst	monoclinic	triclinic	monoclinic
space group	$C2/c$	$P\bar{1}$	$P2_1/n$
a (Å)	13.434(3)	10.5620(3)	13.8426(9)
b (Å)	12.594(3)	11.8290(5)	28.9003(16)
c (Å)	21.626(4)	13.2190(5)	14.5237(9)
α (deg)	90	81.200(2)	90
β (deg)	99.95(3)	87.030(2)	100.956(4)
γ (deg)	90	75.373(2)	90
V (Å^3)	3604.0(12)	1579.07(10)	5704,4(6)
Z	4	2	6
calcd density (g/cm^3)	1.558	1.566	1,557
μ (mm^{-1})	1.397	1.582	1,321
F(000)	1744	776	2736
T (K)	120(2)	110(2)	120(2)
θ range (deg)	2.23−25.99	3.12−27.55	2.01−25.06
no. of rflns collected	18 867	28 433	59 059
no. of unique rflns	3541	7188	10 034
R_{int}	0.0443	0.0468	0.2414
R1/wR2* ($I > 2\sigma(I)$)	0.0300/0.0604	0.0376/0.0773	0.0771/0.1720
R1/wR2* (all data)	0.0496/0.0656	0.0608/0.0852	0.1820/0.2204
GOF	1.045	1.026	1.020

graphite-monochromated Mo Kα radiation (λ = 0.710 73 Å). The data were corrected for Lorentz−polarization effects and for the effects of absorption (analytical method using a multifaceted crystal model). The structures were solved by direct methods and refined by full-matrix least-squares methods on F^2 using the SHELX-97 set of programs.[19] CCDC reference numbers: 676177−676179.

Results and Discussion

A set of five pyrazolate-based dinucleating ligands, $\mathbf{H_3L^1}$−$\mathbf{H_3L^5}$, was used in the present study (Scheme 1). The ligands differ in the chelating side arms at the 3- and 5-positions of the heterocycle. $\mathbf{H_3L^1}$ is asymmetric, with two different side arms, while $\mathbf{HL^2}$−$\mathbf{H_3L^5}$ each provide two identical compartments.

Reactions of the ligands with 1 equiv of zinc salts in methanol or DMF were accompanied by deprotonation of the N−H pyrazole moieties (and also by deprotonation of the carboxylic and oxime groups in the corresponding ligands) and resulted in formation of 2:2 species, which was confirmed by ESI-MS monitoring of the reaction mixtures. The corresponding binuclear neutral and cationic zinc(II) complexes were isolated by slow evaporation of the reaction solutions at room temperature in the air or under an atmosphere of pyridine vapor (in the case of **1**), which acts as a base and a coligand. The complexes have been isolated and fully characterized, including single-crystal X-ray crystallography (with the exception of **3**). In all cases, two zinc ions are hosted within the adjacent compartments of two opposing ligand strands and are doubly bridged by the two pyrazolates.

For complexes **1**, **3**, and **4** with the oxime-containing ligands, infrared absorption peaks assigned to the ν(N−O) stretching mode of the oxime groups were found to be noticeably shifted to higher frequencies as compared to the spectra of the corresponding free ligands ($\Delta\nu$ = 35 (**1**), 27 (**3**), 157 and 140 cm^{-1} (**4**)). This clearly suggests coordination of the oxime group via the nitrogen atom, as observed in the solid-state structures of **1** and **4** (see below).[20,21]

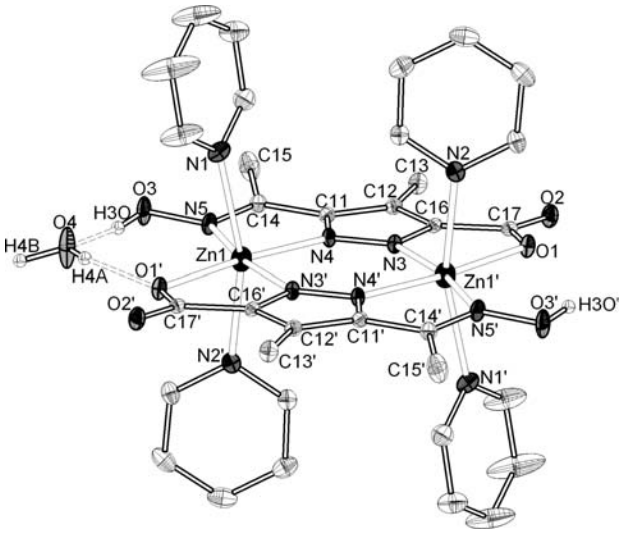

Figure 1. View of the molecular structure of **1**. In the interest of clarity, all protons except those of the H_2O bridge have been omitted.

Structural Characterization of Complexes. According to X-ray crystallography, crystals of **1** consist of the dinuclear neutral complex molecules $[Zn_2(\mathbf{HL^1})_2Py_4]$ and water solvate molecules (Figure 1; selected interatomic distances and angles are given in Table 2). The complex species is a centrosymmetric dimer; the inversion center is located at the midpoint of a segment which connects two zinc atoms. The distance Zn(1)···Zn(1′) (the prime indicates the symmetry transformation 1.5 − x, 0.5 − y, 1 − z) is 4.1145(9) Å. The complex comprises two zinc(II) ions and two trans-disposed doubly

(19) Sheldrick, G. M. *SHELX97, Programs for Crystal Structure Analysis (Release 97-2)*; Universität Göttingen, Göttingen, Germany, **1998**.

(20) Onindo, Ch. O.; Sliva, T. Yu.; Kowalk-Jankowska, T.; Fritsky, I. O.; Buglyo, P.; Petti, L. D.; Kozłowski, H.; Kiss, T. *J. Chem. Soc., Dalton Trans.* **1995**, 3911–3915.

(21) Barjesteh, H.; Chakrabarti, J.; Charalambous, J.; Carugo, O.; Castellani, C. B. *Polyhedron* **1996**, *15*(8), 1323–1330.

Table 2. Selected Interatomic Distances (Å) and Angles (deg) for **1**[a]

Zn(1)−O(1)	2.1602(16)	Zn(1)−N(5)	2.335(2)
Zn(1)−N(1)	2.208(2)	Zn(1)···Zn*(1)	4.114
Zn(1)−N(2)	2.1744(19)	O(3)−N(5)	1.395(2)
Zn(1)−N(3)	2.0686(18)	N(3)−N(4)	1.335(2)
Zn(1)−N(4)	2.0473(18)		
O(1)−Zn(1)−N(1)	86.82(7)	N(3)−Zn(1)−N(2)	94.68(7)
O(1)−Zn(1)−N(2)	85.42(7)	N(3)−Zn(1)−N(5)	167.01(7)
O(1)−Zn(1)−N(5)	116.21(6)	N(4)−Zn(1)−O(1)	171.57(6)
N(1)−Zn(1)−N(5)	84.00(7)	N(4)−Zn(1)−N(1)	95.67(7)
N(2)−Zn(1)−N(1)	161.83(7)	N(4)−Zn(1)−N(2)	94.37(7)
N(2)−Zn(1)−N(5)	84.73(7)	N(4)−Zn(1)−N(3)	95.02(7)
N(3)−Zn(1)−O(1)	76.61(6)	N(4)−Zn(1)−N(5)	72.12(7)
N(3)−Zn(1)−N(1)	99.47(7)		

[a] Symmetry transformations used to generate equivalent atoms: (*) $-x+{}^{3}/_{2}, -y+{}^{1}/_{2}, -z+1$.

deprotonated pyrazolate ligands occupying the equatorial positions of the coordination sphere of the metal ions, and this central core is roughly planar (with maximum deviations for non-hydrogen atoms, excluding C-4 methyl carbons, reaching 0.078(2) Å). The pyrazole ring and the carboxylic group of $\mathbf{H_3L^1}$ are ionized, while the oxime group remains protonated. Overall the zinc(II) atom is situated in a distorted-octahedral environment: the equatorial plane is formed by two pyrazolate N atoms from the two different ligand strands (d(Zn−N) = 2.0473(18)−2.0686(18) Å), the oxime N atom of one ligand (d(Zn−N) = 2.335(3) Å), and the carboxylic O atom of the other ligand (d(Zn−O) = 2.160(1) Å). The equatorial plane is only very slightly distorted, with the maximum deviation of the donor atoms from the mean plane not exceeding 0.03(1) Å (for N(3)), while the Zn atom deviates from this plane by 0.136(7) Å. The axial positions at zinc are occupied by the pyridine ligands (d(Zn−N) = 2.175(2)−2.208(2) Å).

Each zinc atom in **1** forms two five-membered chelate rings with the two trans-located ligands: with participation of the carboxylic oxygen of one ligand (Zn(1)−O(1′)−C(17′)−C(16′)−N(3′)) exhibiting an envelope conformation, and with participation of the oxime nitrogen from the other ligand (Zn(1)−N(5)−C(14)−C(11)−N(4)) possessing a planar conformation. A central six-membered bimetallic cycle is formed by two zinc(II) atoms and the two *N*,*N*′-pyrazolate bridges. The virtually planar structure is additionally stabilized by formation of two hydrogen bonds between the water molecule and the carboxylic O atom of the first ligand (O(3)−H(3O) = 0.84 Å, H(3O)···O(4) = 1.82 Å, O(3)−H(3O)···O(4) = 2.644(2) Å, 167.2°) and the oxime OH function of the second ligand (O(4)−H(4A) = 0.92 Å, H(4A)···O(1′) = 1.91 Å, O(4)−H(4A)···O(1′) = 2.750(2) Å, 150.7°). The resulting seven-membered rings (Zn(1)−O(1′)−H(4A)−O(4)−H(3O)−O(3)−N(5)) thus connect the equatorial coordination sphere into a closed pseudomacrocyclic structure.

The crystal structure of **2** consists of the binuclear neutral complex molecules $[Zn_2(\mathbf{L^2})_2(CH_3COO)_2]$ and some molecules of DMF and water of solvation (Figure 2; selected interatomic distances and angles are given in Table 3). Although $[\mathbf{L^2}]^-$ is a symmetric pyrazolate ligand, the complex **2** (unlike **1**) is not centrosymmetric and does not possesses any intrinsic crystallographic symmetry; it only approaches approximate C_{2v} molecular

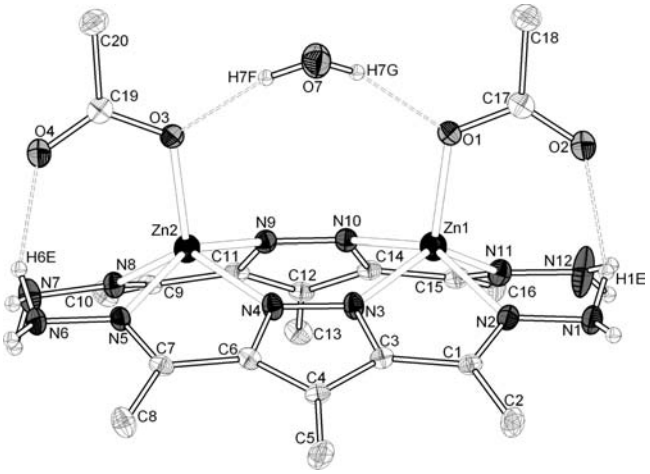

Figure 2. View of the molecular structure of **2**. In the interest of clarity, all protons, except those of the H_2O bridge, have been omitted.

Table 3. Selected Interatomic Distances (Å) and Angles (deg) for **2**

Zn(1)−O(1)	1.9656(17)	Zn(2)−N(9)	2.065(2)
Zn(1)−N(2)	2.210(2)	Zn(1)···Zn(2)	4.094
Zn(1)−N(3)	2.064(2)	N(1)−N(2)	1.395(3)
Zn(1)−N(10)	2.072(2)	N(3)−N(4)	1.343(3)
Zn(1)−N(11)	2.164(2)	N(5)−N(6)	1.395(3)
Zn(2)−O(3)	1.9613(17)	N(7)−N(8)	1.409(3)
Zn(2)−N(4)	2.052(2)	N(9)−N(10)	1.340(3)
Zn(2)−N(5)	2.195(2)	N(11)−N(12)	1.391(3)
Zn(2)−N(8)	2.152(2)		
O(1)−Zn(1)−N(2)	105.14(7)	O(3)−Zn(2)−N(4)	111.76(8)
O(1)−Zn(1)−N(3)	112.32(8)	O(3)−Zn(2)−N(5)	103.84(7)
O(1)−Zn(1)−N(10)	103.70(8)	O(3)−Zn(2)−N(8)	114.70(8)
O(1)−Zn(1)−N(11)	110.07(8)	O(3)−Zn(2)−N(9)	104.47(8)
N(3)−Zn(1)−N(2)	73.88(8)	N(4)−Zn(2)−N(5)	74.36(8)
N(3)−Zn(1)−N(10)	90.46(8)	N(4)−Zn(2)−N(8)	133.51(8)
N(3)−Zn(1)−N(11)	137.47(9)	N(4)−Zn(2)−N(9)	90.64(8)
N(10)−Zn(1)−N(2)	150.69(8)	N(8)−Zn(2)−N(5)	95.78(8)
N(10)−Zn(1)−N(11)	76.39(8)	N(9)−Zn(2)−N(5)	151.28(8)
N(11)−Zn(1)−N(2)	98.33(8)	N(9)−Zn(2)−N(8)	76.71(8)

symmetry. In contrast to the case for **1**, the zinc(II) atoms are situated in a distorted-tetragonal-pyramidal coordination environment of four N atoms (two belonging to the pyrazolate rings and two from the hydrazone N atoms of two different ligands (d(Zn−N) = 2.052(2)−2.210(2) Å)) forming the equatorial plane and the O atom of the monodentately coordinated acetate group (d(Zn−O) = 1.9613(17) and 1.9656(17) Å) occupying the apical position. The Zn···Zn separation (4.094(7) Å) is very close to that observed in **1**, while the conformation of the complex noticeably differs from that in **1**: both pyrazolate ligands are significantly tilted from a coplanar disposition with a dihedral angle of 122.4° between their mean planes defined by the non-hydrogen atoms. Thus, the conformation of the binuclear complex may be described as a "rooflike" structure, crowned by two "antennas" of the acetate anions. The zinc atoms are significantly displaced from the mean plane defined by the four equatorial donor atoms in the direction of the acetate ions (by 0.649 and 0.676 Å for Zn(1) and Zn(2), respectively). The six-membered bimetallic cycle exhibits a boat conformation (Zn(1) and Zn(2) atoms displaced from the N(3)N(4)N(9)N(10) mean plane by 0.455 and 0.471 Å, respectively).

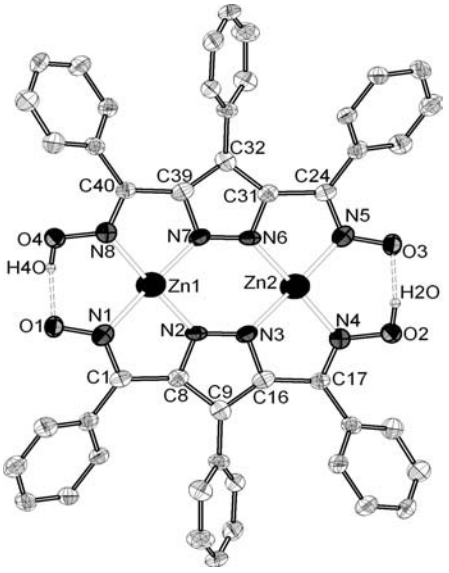

Figure 3. View of the molecular structure of **4**. In the interest of clarity, all protons except H(2O) and H(4O) have been omitted.

The most interesting feature of this structure is the additional support of apical monodentate acetate coordination by intramolecular hydrogen bonds that form between the uncoordinated acetate O atoms and the amine N atom of the hydrazone groups as well as between the coordinated acetate O atom and a single water molecule located above the central six-membered bimetallic cycle (Figure 2). Thus, the water molecule bridges two acetate anions by acting as a 2-fold hydrogen bond donor. These hydrogen bonds supporting the acetate coordination and the bridging function of the central water molecule may be very important features with respect to substrate interaction with the bimetallic active site of zinc hydrolytic enzymes. It demonstrates the possibility of efficient substrate binding by the synergetic effects of both metal−ligand bonds and hydrogen bonds, which is reminiscent of the more complex enzyme−substrate interactions in natural systems. Moreover, the bridging role of the water molecule may facilitate simultaneous binding of two substrate molecules to the active site, which should be taken into account when employing substrates that have relatively small interdonor distances, not suitable to provide a good fit for bridging coordination of one substrate molecule at a binuclear site. Indeed, the O···O separation in acetate (2.226 Å) is too short for unstrained bridging coordination in **2**, while in phosphate and phosphoesters this separation is much longer, which is a prerequisite for bridging coordination to bimetallic sites with metal−metal separations of around 4 Å.

The molecular structure of **4** is presented in Figure 3; selected interatomic distances and angles are given in Table 4. The structure consists of the neutral binuclear complex molecules $[Zn_2(\mathbf{HL}^4)_2]$ containing two doubly deprotonated ligands coordinated to two zinc(II) ions. The unit cell contains two crystallographically independent molecules that insignificantly differ in their geometrical and conformational parameters: (1) molecules containing two crystallographically independent zinc atoms (d(Zn(1)···Zn(2))=3.761 Å); (2) centrosymmetric

Table 4. Selected Interatomic Distances (Å) and Angles (deg) for **4**

Zn(1)−N(2)	1.837(7)	Zn(3)−N(11)	1.894(8)
Zn(1)−N(7)	1.855(7)	Zn(3)···Zn(3′)	3.750
Zn(1)−N(8)	1.863(7)	O(1)−N(1)	1.330(9)
Zn(1)−N(1)	1.889(8)	O(2)−N(4)	1.338(9)
Zn(2)−N(3)	1.834(7)	O(4)−N(8)	1.335(9)
Zn(2)−N(6)	1.854(7)	O(5)−N(9)	1.342(9)
Zn(2)−N(5)	1.869(8)	O(6)−N(11)	1.297(9)
Zn(2)−N(4)	1.902(8)	N(2)−N(3)	1.320(9)
Zn(1)···Zn(2)	3.761	N(6)−N(7)	1.322(10)
Zn(3)−N(12)	1.815(7)	N(10)−N(12′)	1.318(10)
Zn(3)−N(10)	1.841(7)	N(12)−N(10′)	1.318(10)
Zn(3)−N(9)	1.886(7)		
N(2)−Zn(1)−N(1)	82.0(3)	N(3)−Zn(2)−N(4)	81.6(3)
N(2)−Zn(1)−N(7)	96.7(3)	N(6)−Zn(2)−N(4)	175.8(3)
N(2)−Zn(1)−N(8)	174.5(3)	N(5)−Zn(2)−N(4)	99.1(3)
N(7)−Zn(1)−N(1)	174.8(3)	N(9)−Zn(3)−N(11)	100.6(3)
N(7)−Zn(1)−N(8)	81.8(3)	N(10)−Zn(3)−N(9)	81.1(3)
N(8)−Zn(1)−N(1)	99.0(3)	N(10)−Zn(3)−N(11)	178.3(3)
N(3)−Zn(2)−N(6)	96.3(3)	N(12)−Zn(3)−N(9)	177.4(3)
N(3)−Zn(2)−N(5)	175.5(3)	N(12)−Zn(3)−N(10)	96.6(3)
N(6)−Zn(2)−N(5)	82.7(3)	N(12)−Zn(3)−N(11)	81.7(3)

dimers (the Zn(3)···Zn(3′) distance (the prime indicates the symmetry transformation $-x$, $-y$, $-z$) is 3.750 Å). Note that these separations are much shorter than those observed in **1** and **2**. Interestingly, in both types of molecules the metal atoms exhibit a lower coordination number than in **1** and **2** and are found in a distorted-square-planar coordination environment provided by the two pyrazolate nitrogen atoms and two oxygen atoms belonging to the deprotonated oxime group of one of the ligands (d(Zn−N) = 1.863(7)−1.886(7) Å) and the protonated oxime group of the second ligand (d(Zn−N) = 1.889(8)−1.894(8) Å). A likely reason for the lower coordination number in **4** is the presence of six bulky phenyl rings that provide a hydrophobic periphery of the complex, thus disfavoring occupation of apical positions by monodentate ligands. The pyrazolate ligand strands in **4** appear to be closed into a pseudomacrocyclic framework via intramolecular hydrogen bonds between the oxime oxygen atoms of the protonated and ionized oxime groups from two opposite ligand arms, which is typical for bis(oximato) complexes: O(4)−H(4O) = 0.85 Å, H(4O)···O(1) = 1.71 Å, O(4)−H(4O)···O(1) = 2.461(8) Å, 146.4°; O(2)−H(2O) = 0.85 Å, H(2O)···O(3) = 1.71 Å, O(2)−H(2O)···O(3) = 2.510(9) Å, 155.3°; O(5)−H(5O) = 0.85 Å, H(5O)···O(6) = 1.67 Å, O(5)−H(5O)···O(6) = 2.511(9) Å, 168.2°).

Each metal atom in **4** forms two five-membered, almost planar chelate rings with the ligands (Zn−N−C−C−N). In the case of type 1 molecules, the central six-membered bimetallic cycle adopts a boat conformation (similar to the case for compound **2**). This is due to the fact that the ligands are not located in the same plane (the dihedral angle between the pyrazole ring planes is 149°, and the zinc atoms are displaced from the N(2)−N(3)−N(6)−N(7) mean plane by 0.136 and 0.147 Å for Zn(1) and Zn(2), respectively). In the case of type 2 molecules, the six-membered bimetallic cycle adopts a planar conformation (similar to compound **1**). This suggests that the bimetallic array exhibits some flexibility and interconversion between the planar and boat conformations is obviously facile.

5 was previously reported;[17] the Zn···Zn separation in **5** is close to that in **1** and **2** (4.015 Å). Thus, the

Table 5. Protonation Constants of the Ligands $\mathbf{H_3L^5}$ and $\mathbf{H_3L^1}$ and Complex Stability Constants with Zinc at 25 °C and 0.1 M ($NaClO_4$)

	$\mathbf{H_3L^1}$			$\mathbf{H_3L^5}$	
species	$\log\beta$	pK_a	species	$\log\beta$	pK_a
$[\mathbf{H_4L}]^+$	7.62(2)	1.94	$[\mathbf{H_4L}]^+$	11.85(5)	1.64
$[\mathbf{H_3L}]$	5.672(9)	5.67	$\mathbf{H_3L}$	10.21(1)	4.38
$[Zn\mathbf{H_2L}]^+$	4.16(2)		$[\mathbf{H_2L}]^-$	5.83(1)	5.83
$[Zn_2\mathbf{H_2L}_2]^0$	−1.85(6)	6.83	$[Zn\mathbf{H_2L}]^+$	9.76(2)	
$[Zn_2\mathbf{HL}_2]^-$	−8.68(6)	8.32	$[Zn_2\mathbf{H_2L}_2]^0$	15.14(3)	
$[Zn_2\mathbf{L}_2]^{2-}$	−17.00(9)		$[Zn_2\mathbf{L}_2]^{2-}$	6.13(5)	

intermetallic distances in the present series of binuclear complexes fall well within the range typically encountered in dinuclear zinc sites of natural hydrolases (e.g., alkaline phosphatase, $d(Zn\cdots Zn) = 4.0$ Å),[22] and cooperative effects in hydrolytic substrate transformations can thus be expected. Interestingly, coordination numbers of the zinc ions in these complexes vary from 4 to 6 and seem to be quite sensitive to the structural features of the coordinated pyrazolate ligands and the nature of the peripheral groups, which is a prerequisite for easy changes of coordination numbers in the course of catalytic cycles.

Species in Solution. While the X-ray crystallographic results provide structural insights for the various complexes in the solid state, the species distribution in solution is crucial for understanding any hydrolytic reactivity. Potentiometric titrations were performed to determine the pK_a values of the ligands, as well as the stability constants of their zinc complexes (Table 5).

Ligand Protonation Constants. In the case of $\mathbf{H_3L^5}$ three protonation constants were obtained; two ionizable protons belong to the carboxylate groups ($pK_{a3} = 5.83$, $pK_{a2} = 4.38$). Furthermore, the pyrazole moiety may become protonated to give $[\mathbf{H_4L^5}]^+$ ($pK_{a1} = 1.64$). $[\mathbf{H_4L^1}]^+$ behaves as a dibasic acid with protonation constants corresponding to the pyrazole ($pK_{a1} = 1.94$) and carboxylate functions ($pK_{a2} = 5.67$). Note that in both ligands the pK_a values of the carboxylic groups are much higher than the values observed in the related pyridine carboxylic acids (e.g., for 2,6-dipicolinic acid $pK_{a1} = 2.09$, $pK_{a2} = 4.53$),[23] which reflects the π-donor nature of the pyrazole ring. Also, the observation of only two deprotonation steps for $[\mathbf{H_4L^1}]^+$ with a standard potentiometric protocol implies that the third and fourth protonation constants that could be attributed to the oxime and the pyrazole groups must be higher than 12. For comparison, pK_{a2} of the oxime group in 2-hydroxyiminopropanoic acid is 11.608(7).[20]

The ligands $\mathbf{HL^2}$, $\mathbf{H_3L^3}$, and $\mathbf{H_3L^4}$ and their zinc complexes could not be investigated potentiometrically due to the lack of proton dissociations within the pH range studied.

Species Distribution of Zinc Complexes. The calculations based on the potentiometric data have shown that $\mathbf{H_3L^5}$ forms $[Zn\mathbf{H_2L^5}]^+$, $[Zn_2\mathbf{HL^5}_2]$, and $[Zn_2\mathbf{L^5}_2]^{2-}$ species, while for $\mathbf{H_3L^1}$ four species are formed: $[Zn\mathbf{H_2L^1}]^+$ and dimeric $[Zn_2\mathbf{H_2L^1}_2]$, $[Zn_2\mathbf{HL^1}_2]^-$, and $[Zn_2\mathbf{L^1}_2]^{2-}$. Above pH 7 only dimeric complexes are present, $[Zn_2\mathbf{L^5}_2]^{2-}$ for $\mathbf{L^5}$ and $[Zn_2\mathbf{HL^1}_2]^-$ and $[Zn_2\mathbf{L^1}_2]^{2-}$ for $\mathbf{L^1}$, some of which may be involved in the hydrolysis processes discussed below.

The cationic species $[Zn\mathbf{H_2L^5}]^+$ involves in coordination the carboxylate O atom of one of the deprotonated carboxylic groups and the N-donor of the neutral pyrazole ring. This species exists only in acidic solution, with maximum abundance (nearly 60%) at pH 3.5. Above pH 3.5 the binuclear neutral species $[Zn_2\mathbf{HL^5}_2]$ appears, reaching its maximum abundance of more than 60% at pH 4.3. At even higher pH cooperative deprotonation of the carboxylic groups facilitates the formation of the binuclear anionic species $[Zn_2\mathbf{L^5}_2]^{2-}$, which is dominant above pH 4.5 and the only complex species in the pH range used for all hydrolysis experiments. It reaches 100% abundance at pH ~6, and no additional deprotonation occurs with further increase of pH.

$[Zn\mathbf{H_2L^1}]^+$ with the carboxylate deprotonated is predominating up to a pH of around 6, while binuclear complexes dominate above pH 6.5. Dimer formation involves deprotonation and binding of both pyrazole N as well as coordination of the oxime N. According to the complex speciations (Figure 4) above pH 7 only binuclear complexes are present, suggesting that binuclear structures are responsible for the catalytic activity. The first-formed binuclear species, $[Zn_2\mathbf{H_2L^1}_2]$, is neutral, and its maximum abundance is less than 40% at pH 6.75, as the anionic species $[Zn_2\mathbf{HL^1}_2]^-$ starts to form with a delay of only ca. 0.5 pH units. The two sequential deprotonation steps with pK values of 6.83 and 8.32 can be assigned to proton release from axially coordinated water molecules, resulting in the formation of hydroxo species, and hence $[Zn_2\mathbf{HL^1}_2]^-$ should be better described as $[Zn_2\mathbf{HL^1}_2(OH)]^-$. We also considered the possibility of deprotonation of the oxime group in these species but rejected it as unlikely. Indeed, deprotonation of the axially coordinated water molecule in zinc(II) complexes can occur at pH 7−8. For example, ionization of the

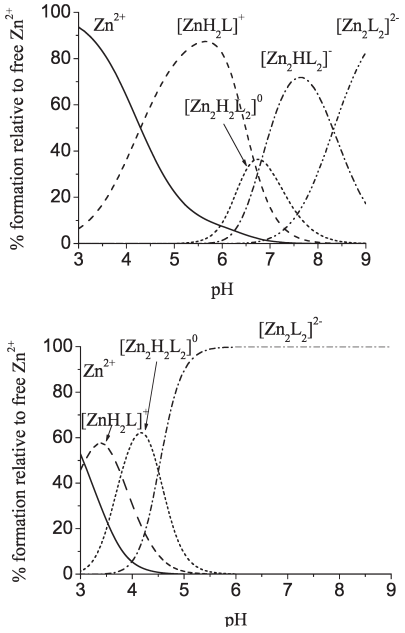

Figure 4. Species distribution diagrams for the $Zn/\mathbf{H_3L^1}$ (top) and $Zn/\mathbf{H_3L^5}$ (bottom) systems ($c_L = 2 \times 10^{-3}$ M and $c_{Zn} = 1 \times 10^{-3}$ M, where c_L = total ligand concentration and c_{Zn} = total concentration of zinc).

(22) Stec, B.; Holtz, K. M.; Kantrowitz, E. R. *J. Mol. Biol.* **2000**, *299*(5), 1303–1311.
(23) Napoli, A. *Talanta* **1968**, *15*(2), 189–198.

axially coordinated water molecule was observed in five-coordinated and tetrahedral zinc complexes with the macrocyclic ligands 1,4,7,10-tetraazacyclododecane and 1,5,9-triazacyclododecane, where it occurs with pK_a = 7.9 and 7.3, respectively.[24] A slightly decreased value of the first pK (6.83) can be explained by the stabilizing effect of an intramolecular H-bond pattern formed by the hydroxyl with the axial water molecule of the second zinc ion, possibly via a bridging water molecule, similar to the situation observed in the structure of **2**. This H-bond can also facilitate the deprotonation of the second axial water molecule with a pK value only 1.5 orders of magnitude higher than the first one.

As we mentioned above, we discounted the possiblitity of ionization of the oxime group upon formation of the anionic species to give $[Zn_2\mathbf{HL^1}_2]^-$ as very unlikely: dissociation of the proton in $[Zn_2\mathbf{HL^1}_2]$ occurs with a pK_a value of less than 7: i.e., more than 5 orders of magnitude lower than in the free ligand. As a rule, if the oxime group is not involved in the formation of any N−O bridges, pK_a values of the N-coordinated oxime groups do not change significantly in the metal complexes as compared to the free ligands. For example, deprotonation of the oxime group in cationic 1:2 zinc complexes with 2-aminoacetamidoxime and 2-(methylamino)acetamidoxime proceeds with pK_a values of 8.71 and 8.54, respectively.[25] These values are even higher than the pK_a values of the oxime groups in the free ligands (7.94 and 8.26, respectively). In $\mathbf{H_3L^1}$ the pK_a value of the oxime group must be higher than 12 (see above). In the case of $[Zn_2\mathbf{HL^1}_2]$ the involvement of the oxime proton in the formation of a hydrogen bond with a bridging water molecule and the deprotonated carboxylic group, as observed in **1**, will be also a factor significantly impeding oxime ionization, thus contributing to a relatively high pK_a (Scheme 3). We have also shown in a series of papers dealing with complex formation of oxime ligands that oxime protons are not ionized if they are involved in intramolecular hydrogen bonds that result in the formation of pseudomacrocyclic closed structures, and the corresponding pK_a values are much higher than 7.[26] In contrast, deprotonation of axially coordinated water from the neutral species with a pK_a value of around 7 appears reasonable and is in agreement with literature data. The second deprotonation with pK_a 8.32 may be attributed either to the deprotonation of the second axial water or to the deprotonation of the oxime group. We think that the former is much more likely, as both coordinated hydroxyls on the adjacent zinc atoms can be linked via the bridging water molecule to form hydrogen bonds (as observed in the structure of **2**). Note that, unlike the $\mathbf{L^1}$-containing bimetallic species, the $[Zn_2\mathbf{L^5}_2]^{2-}$ complex discussed above does not undergo ionization of axial water over the measured pH range.

Scheme 3. Possible Structure of the Anionic Species $[Zn_2\mathbf{L^1}_2]^{2-}$

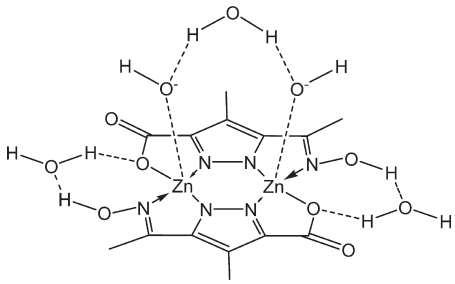

This important difference is understandable in terms of the anionic nature of the species $[Zn_2\mathbf{L^5}_2]^{2-}$, bearing a double negative charge, whereas $[Zn_2\mathbf{H_2L^1}_2]$ is a neutral species.

Complex formation in solution has also been studied by ^{1}H NMR. Disappearance of the signal for the pyrazole NH proton is in accordance with potentiometric results.

Phosphate Ester Hydrolysis. Paraoxon-ethyl (POE) and 2-(hydroxypropyl)-*p*-nitrophenyl phosphate (HPNP) were used as substrates in this study. Cleavage of these phosphate ester bonds and liberation of 4-nitrophenolate can be easily monitored by the strong absorption of the latter at 414 nm. Zn-mediated hydrolytic reactions, including phosphatase-like activity, are best studied in buffered aqueous solution (or in media with high water content) in order to most closely mimic biological conditions. In order to exclude any effects from different (and potentially coordinating) counteranions in the comparative reactivity studies, the perchlorate salts were used for all complexes. An initial screening of the hydrolytic activities of the various complexes was carried out at pH 8.50 for POE and pH 8.00 for HPNP in DMSO/buffered water (1:1) at 50 °C. These conditions roughly correspond to the maximum hydrolysis rates of the substrates, as follows from the bell-shaped pH profiles (Figure 5 and 6).

The kinetic data for all complexes show that the rate of hydrolysis of POE and HPNP is linearly dependent on the complex concentration. Pseudo-first-order rate constants k_{obs} (defined by $v_0 = k_{obs}[complex]_0$) are shown in Charts 1 and 2 and follow the order **3** > **1** > **5** ≈ **2** for paraoxon-ethyl and **2** > **3** > **5** ≈ **1** for 2-(hydroxypropyl)-*p*-nitrophenyl phosphate. Complex **4** has not been tested, because it is not soluble in the mixture DMSO/buffered water (1:1). The hydrolysis of both substrates was also tested in the presence of free zinc(II) ions only under the conditions corresponding to those applied in all experiments. The control experiment gave k_{obs} values much lower than those for complex-promoted hydrolysis (Table 6).

The dependence of the initial rate of hydrolysis on substrate concentration (Figures 7 and 8) shows that the reaction is first order in POE and HPNP at low concentrations. For many catalyst/substrate pairs, the concentration dependence remains linear at higher substrate concentrations as well, indicating an overall second-order rate law:

$$V = k_2[complex][S]$$

and $V_0 = k_2[complex]_0[S_0]$ where S denotes the substrate (POE or HPNP).

(24) Koike, T.; Takamura, M.; Kimura, E. *J. Am. Chem. Soc.* **1994**, *116*, 8443–8449.

(25) Orama, M.; Saarinen, H.; Raikas, T.; Korvenranta, J. *Finn. Chem. Lett.* **1986**, *13*(3), 59–63.

(26) (a) Duda, A. M.; Karaczyn, A.; Kozłowski, H.; Fritsky, I. O.; Głowiak, T.; Prisyazhnaya, E. V.; Sliva, T. Yu.; Świątek-Kozłowska, J. *J. Chem. Soc., Dalton Trans.* **1997**, *20*, 3853–3859. (b) Dobosz, A.; Dudarenko, N. M.; Fritsky, I. O.; Głowiak, T.; Karaczyn, A.; Kozłowski, H.; Sliva, T. Yu.; Swiatek-Kozlowska, J. *J. Chem. Soc., Dalton Trans.* **1999**, *5*, 743–749.

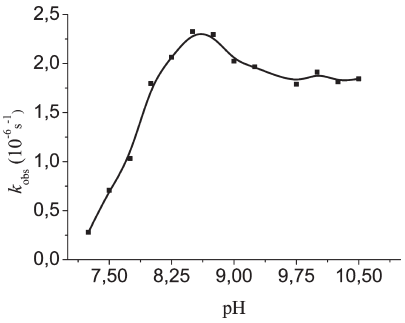

Figure 5. Effect of pH on POE hydrolysis rate mediated by **1**. Conditions: $[\mathbf{1}]_0 = 0.8$ mM, $[POE]_0 = 1.6$ mM, at 50 °C, in DMSO/buffered H_2O (1:1).

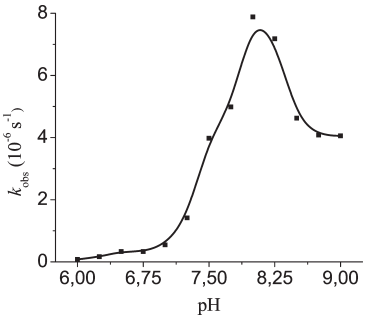

Figure 6. Effect of pH on HPNP hydrolysis rate mediated by **1**. Conditions: $[\mathbf{1}]_0 = 0.8$ mM, $[HPNP]_0 = 1.6$ mM, at 50 °C, in DMSO/buffered H_2O (1:1).

Chart 1. k_{obs} for POE Hydrolysis Promoted by **1**, **2**, **3**, and **5** and Self-Cleavage[a]

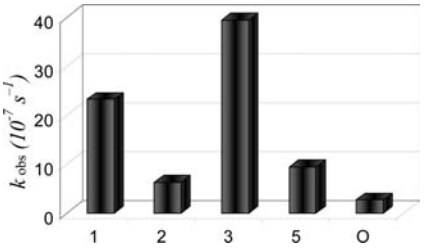

[a] Conditions: $[POE]_0 = 2$ mM, at 50 °C, pH 8.50, in DMSO/TAPS buffer (1:1).

Chart 2. k_{obs} for HPNP Hydrolysis Promoted by **1**, **2**, **3**, and **5** and Self-Cleavage[a]

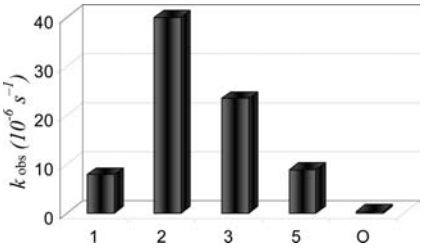

[a] Conditions: $[HPNP]_0 = 2$ mM, at 50 °C, pH 8.00, in DMSO/TAPS buffer (1:1).

However, for some complexes (compound **1** for POE and **5** for HPNP), a decrease in the reaction rate at higher substrate concentration was observed (Figure 7), indicating saturation behavior. This can be explained in terms of a substrate-binding pre-equilibrium which is reminiscent

Table 6. Kinetic Data k_{obs} (s^{-1}) for POE and HPNP Hydrolysis Promoted by free Zinc(II) at 50 °C and at pH 8.50 and 8.00, Respectively, in DMSO/Buffered Water (1:1)

	POE	HPNP
Zn^{2+}	2.97×10^{-7}	9.21×10^{-7}

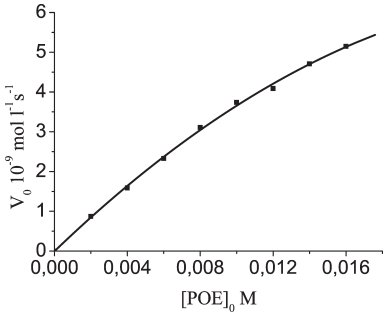

Figure 7. Dependence of the initial rate of POE hydrolysis mediated by **1** on substrate concentration. Conditions: $[\mathbf{1}]_0 = 0.4$ mM, at 50 °C, pH 8.50, in DMSO/TAPS buffer (1:1).

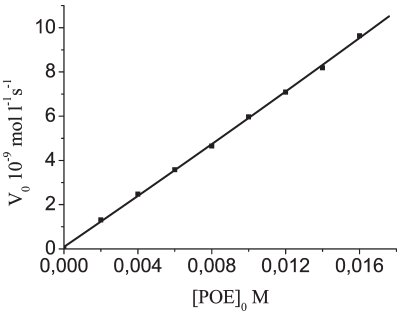

Figure 8. Dependence of the initial rate of POE hydrolysis mediated by **2** on substrate concentration. Conditions: $[\mathbf{2}]_0 = 0.4$ mM, at 50 °C, pH 8.50, in DMSO/TAPS buffer (1:1).

of the Michaelis−Menten behavior typical of native metalloenzymes:

$$\text{complex} + \text{S} \underset{k_{-1}}{\overset{k_1}{\Leftrightarrow}} \{\text{complex} - \text{S}\} \overset{k_{cat}}{\Rightarrow} \text{products}$$

Kinetic data that showed the saturation dependence of substrate concentration has been modeled according to the rate law given in eq 1 to yield values for K_M and k_{cat} (Table 7).

$$V_0 = \frac{k_{cat}[\text{complex}]_0[\text{S}]_0}{K_M + [\text{S}]_0} \quad (1)$$

with

$$K_M = \frac{k_{-1} + k_{cat}}{k_1}$$

The value of k_{cat}/K_M is commonly used as a measure of the efficiency of reagents and catalysts which display saturation kinetics; this value can be directly compared to the rate constants, k_2, measured for simple second-order processes (Table 7).

Kinetic results for phosphate ester hydrolysis, viewed together with the speciation of zinc complexes determined by potentiometric titrations, allow us to propose a classical double Lewis acid activation mechanism. The rates of POE or HPNP hydrolysis increase with an increase of pH

Table 7. Kinetic Data k_2 (in M^{-1} s^{-1}; k_{cat}/K_M) for POE and HPNP Hydrolysis Promoted by Zinc(II) Complexes at 50 °C and pH 8.50 and 8.00, Respectively, in DMSO/Buffered Water (1:1)

complex	POE	HPNP
1	1.14×10^{-3}	1.65×10^{-2}
2	1.47×10^{-3}	2.32×10^{-2}
3	1.98×10^{-3}	1.43×10^{-2}
5	1.65×10^{-3}	1.35×10^{-2}

from 4 to 8 (Figures 5 and 6). The following drop in hydrolysis rates above pH 8−8.5 accounts for the bell-shape dependence. Potentiometric titrations demonstrated the preferential existence of dinuclear zinc complexes with ligands $\mathbf{H_3L^1}$ and $\mathbf{H_3L^5}$ under these conditions; it is reasonable to assume that the remaining zinc complexes also adopt dimeric structures in basic media. This assumption is supported by similar structures of zinc complexes with $\mathbf{H_3L^1}$−$\mathbf{H_3L^5}$ in the solid state, by the rather similar catalytic activities of all complexes (Table 7), and by the identical first-order rate law in zinc complexes determined for all hydrolytic reactions in our study. In addition to stabilizing the dinuclear zinc species, a pH increase also causes an increase in the concentration of the nucleophile (free or coordinated hydroxide ions). Deprotonation of coordinated water was clearly detected above pH 7.5 for the system containing zinc(II) and $\mathbf{H_3L^1}$, from both potentiometric (Figure 4A) and kinetic curves (Figures 5 and 6). The bell-shaped plots of k_{obs} vs pH yield pK_a values for **1** equal to 7.2 and 9.2 for POE hydrolysis and 7.3 and 8.5 for HPNP hydrolysis. Those values correspond well to pK_a values for terminally zinc bound hydroxide (Table 5), which therefore can act as a nucleophile in substrate hydrolysis with complex **1**.[27] A high equilibrium concentration of zinc hydroxo species, however, is not a prerequisite for catalytic activity of our pyrazolate complexes. Indeed, complex **5**, which carries a negative charge in alkaline media (due to the trianionic nature of the ligand $\mathbf{H_3L^5}$), does not promote deprotonation of coordinated water (Figure 4B) but still facilitates phosphate ester hydrolysis. Direct comparison of substrate hydrolysis rates promoted by **1** or **5** show slightly (ca. 2-fold) higher activity of **1** (Table 7). It can be concluded that the presence of zinc-bound hydroxide slightly increases the catalytic activity of dizinc complexes supported by pyrazolates, but substrate activation due to its coordination to zinc appears to be the major factor governing the hydrolytic activity of **1**−**5**. It should also be noted that the substrate upon coordination to the dizinc scaffold may replace one or both of the axially bound water/hydroxyl ligands. The shapes of concentration dependence of hydrolysis rates also support this conclusion: full saturation was never achieved for our reactions, and observed reaction rates reflect exclusively (for linear k_{obs} vs [substrate] plots) or predominantly (for curved k_{obs} vs [substrate] plots) the pre-equilibrium step of substrate coordination to the respective dizinc complex. It is not surprising that the series of complexes **1**−**5** displays fairly similar reactivities in hydrolysis of a given substrate, because the structures (geometric and electronic) and accessibility of zinc toward coordination of the incoming phosphoester would be similar throughout this series.

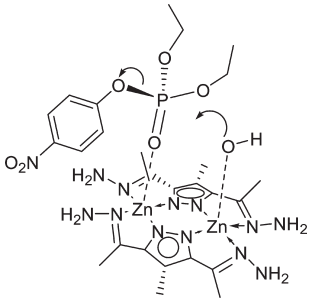

Figure 9. Proposed mechanism of POE hydrolytic cleavage mediated by **2**.

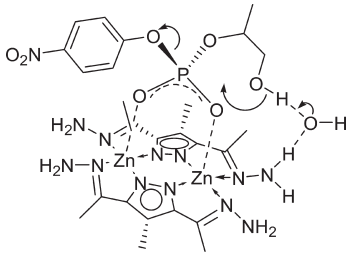

Figure 10. Proposed mechanism of HPNP cyclization mediated by **2**.

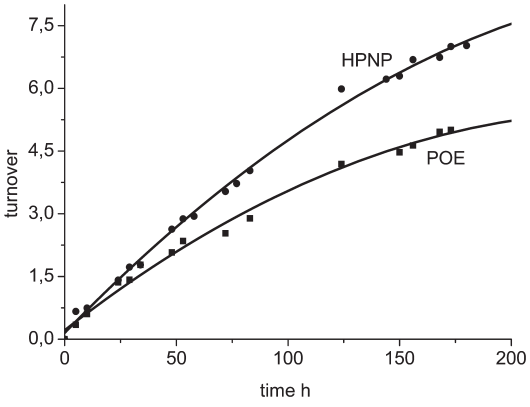

Figure 11. Time course of hydrolytic conversion of POE and HPNP by **1** as monitored by UV−vis spectroscopy. Conditions: pH 8.50 and 8.00, at 50 °C, in DMSO/buffered H_2O (1:1).

When the catalytic effects of the Zn(II) complexes in reactions with different substrates are compared, it can be seen that k_2 for HPNP hydrolysis is about 1 order of magnitude larger than for POE hydrolysis. Meanwhile, rates of the self-cleavage for POE and HPNP are similar. This can be explained in terms of the different natures of substrate activation: HPNP can be coordinated by two zinc ions, but POE likely coordinates to only one zinc ion (Figures 9 and 10). In the case of HPNP the rate of hydrolysis is additionally increased because nucleophilic substitution at the phosphorus atom proceeds in an intramolecular fashion with participation of the hydroxide group of the substrate, resulting in intramolecular cyclization of the phosphodiester. Pseudo-first-order rate constants k_{obs} for the complexes **1**−**3** and **5** show different trends for POE and for HPNP, which can again be attributed to differences in the hydrolytic reaction mechanisms for the substrate cleavage.

(27) Neves, A.; Lanznaster, M.; Bortoluzzi, A. J.; Peralta, R. A.; Casellato, A.; Castellano, E. E.; Herrald, P.; Riley, M. J.; Schenk, G. *J. Am. Chem. Soc.* **2007**, *129*, 7486–7487.

In order to determine whether the complexes act as catalysts for the cleavage of POE and HPNP, reactions in the presence of 20 equiv of the substrates were followed by UV−vis spectroscopy. Turnover was clearly observed: each 1 mol of zinc complex promoted hydrolysis of up to 5 mol of POE and 8 mol of HPNP (Figure 11). A gradual decrease in reaction rate at higher turnover numbers may indicate product inhibition.

Conclusions

Inspired by the dinuclear Zn sites in enzymatic systems, new dinuclear zinc(II) complexes were synthesized and fully characterized using NMR spectroscopy, potentiometry, and X-ray crystallography. These complexes promote significant rate enhancement in the catalytic cyclization of a RNA model substrate, 2-hydroxypropyl-*p*-nitrophenyl phosphate (HPNP), and in the hydrolytic degradation of the pesticide paraoxon-ethyl (POE), over the uncatalyzed reaction with multiple catalyst turnovers.

The mechanism for the hydrolysis of both substrates appears to be classical, involving either a double Lewis acid activation of the bridging phosphoester by two metal ions or the activation of both the substrate and the nucleophile at the two proximate metal ions.

The structural results, together with the kinetic data, suggest that the substrate approaches the complexes and O atoms of POE or HPNP start associating with the two zinc (II) ions of the complex. Simultaneously an OH^- function of the H_2O bridge performs a nucleophilic attack on the phosphorus, followed by the cleavage of the phosphate ester bond. The Zn···Zn separation in all complexes (3.75−4.14 Å) is in a suitable range to allow for bridging substrate coordination in the case of HPNP (compare the metal···metal separation of ∼3.9 Å in alkaline phosphatase). Interestingly, the presence of the oxime groups (or other H-bonding functional groups) in the ligand arms clearly facilitates substrate hydrolysis, which supports the idea that proper H-bonding interactions contribute to the formation of the hydroxide nucleophile. The present binuclear complexes can provide useful model systems for hydrolytic dizinc enzymes, where a bridging coordination of phosphate units has been suggested to play a fundamental role in phosphate ester activation and hydrolysis.

Acknowledgment. Financial support by NATO (Grant No. CBP.NUKR.CLG 982019) and the DFG (International Research Training Group GRK 1422 "Metal Sites in Biomolecules: Structures, Regulation and Mechanisms"; see www.biometals.eu) is gratefully acknowledged. L.V.P. thanks the DAAD (Grant No. GR 6206-A0609168) for a scholarship.

Supporting Information Available: CIF files giving crystallographic data for complexes **1**, **2**, and **4** and text, figures, and a table giving additional information, pH titration curves, and Lineweaver−Burk plots. This material is available free of charge via the Internet at http://pubs.acs.org.